SCIENTIFIC REPORTS
nature research

OPEN

The E3 ubiquitin-protein ligase MDM2 is a novel interactor of the von Hippel–Lindau tumor suppressor

Antonella Falconieri[1,3], Giovanni Minervini[1,3], Raissa Bortolotto[1], Damiano Piovesan[1], Raffaele Lopreiato[1], Geppo Sartori[1], Maria Pennuto[1,2] & Silvio C. E. Tosatto[1]✉

Mutations of the von Hippel–Lindau (pVHL) tumor suppressor are causative of a familiar predisposition to develop different types of cancer. pVHL is mainly known for its role in regulating hypoxia-inducible factor 1 α (HIF-1α) degradation, thus modulating the hypoxia response. There are different pVHL isoforms, including pVHL30 and pVHL19. However, little is known about isoform-specific functions and protein–protein interactions. Integrating in silico predictions with in vitro and in vivo assays, we describe a novel interaction between pVHL and mouse double minute 2 homolog (MDM2). We found that pVHL30, and not pVHL19, forms a complex with MDM2, and that the N-terminal acidic tail of pVHL30 is required for its association with MDM2. Further, we demonstrate that an intrinsically disordered region upstream of the tetramerization domain of MDM2 is responsible for its isoform-specific association with pVHL30. This region is highly conserved in higher mammals, including primates, similarly to what has been already shown for the N-terminal tail of pVHL30. Finally, we show that overexpression of pVHL30 and MDM2 together reduces cell metabolic activity and necrosis, suggesting a synergistic effect of these E3 ubiquitin ligases. Collectively, our data show an isoform-specific interaction of pVHL with MDM2, suggesting an interplay between these two E3 ubiquitin ligases.

Oxygen availability regulates a plethora of physiological processes, such as cell metabolism, mitochondrial ATP production, embryo development and inflammation, and it plays a prominent role in the pathophysiology of cancer[1–3]. Hypoxia response in cells is carried out by the hypoxia-inducible factor (HIF) complex in a tightly oxygen-dependent fashion[4,5]. HIF is a heterodimeric complex formed by an α-subunit, whose stability is finely regulated by the intra-cellular oxygen concentration, and a constitutively expressed nuclear β-subunit[6,7]. As a transcription factor, HIF is a master activator of many genes that allow the cells to cope with low oxygen growth conditions by enhancing glycolytic flux while inhibiting mitochondrial respiration[8]. In physiological conditions, the levels of HIF-1α are regulated by the von Hippel–Lindau (pVHL) tumor suppressor, which continuously targets HIF-1α for proteasomal degradation. As a substrate recognition particle of the VCB multiprotein complex (together with Elongin B, Elongin C, the E3-ubiquitin ligase Cullin-2 and RBX1[9]), pVHL recognizes two proline residues of HIF-1α[10] upon hydroxylation by prolyl hydroxylase domain containing proteins (PHD)[11], whose expression in turn is closely regulated by HIF-1α itself[12]. In hypoxia, the activity of PHDs is inhibited, thus resulting in HIF-1α stabilization and activation of the hypoxia-response gene expression program. Together, pVHL, HIF-1α and PHD form the cellular oxygen-sensing system[4,11,13,14].

Deregulation of HIF-1α/pVHL promotes sustained angiogenesis[15] and is causative of von Hippel–Lindau syndrome[16–18], a familiar predisposition to develop different types of cancer, such as pheochromocytoma, paraganglioma, retinal- and cerebellar-hemangioblastoma, and renal cell carcinoma (RCC)[19]. In humans, the *VHL* gene is located on chromosome 3[20]. Three biologically active pVHL isoforms have been described so far, namely pVHL30, pVHL19, and pVHL172. Both pVHL19 and pVHL30 act as tumor suppressors and have a redundant function to promote HIF-1α degradation, yet they have a different sub-cellular localization[21] and isoform-specific

[1]Department of Biomedical Sciences, University of Padova, Viale G. Colombo 3, 35121 Padua, Italy. [2]Veneto Institute of Molecular Medicine (VIMM), 35129 Padua, Italy. [3]These authors contributed equally: Antonella Falconieri and Giovanni Minervini. ✉email: silvio.tosatto@unipd.it

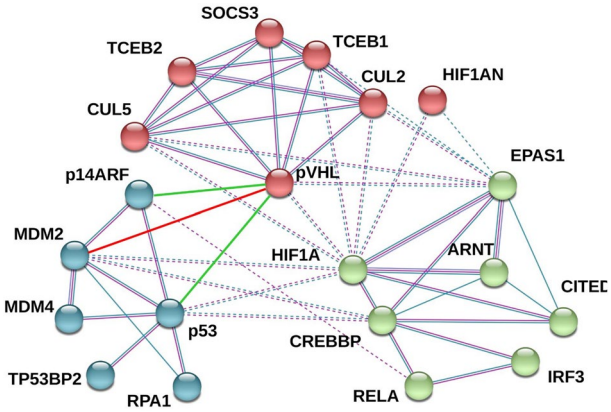

Figure 1. Network of interacting proteins. Connections between nodes represent experimental evidence for interaction, while colored bubbles are for proteins forming the network. A green edge represents the interaction between pVHL30 and p14ARF (CDKN2A), currently not yet reported in STRING, while a red line is used for the novel association of pVHL30 with MDM2 reported here.

functions[9,22]. Conversely, rather than playing a role as tumor suppressor, pVHL172 contributes to renal carcinoma by up-regulating a subset of pro-tumorigenic genes[23], i.e. *Tgfb1*, *Mmp1*, and *Mmp13*. pVHL30 was proposed to specifically interact with p14ARF[22], suggesting a further connection between oxygen sensing and apoptosis. Although these observations suggest that the different pVHL isoforms have redundant as well as isoform-specific functions in the cells, little is known about pVHL isoform-specific protein–protein structural and functional interactions. Here, we report a novel direct interaction between mouse double minute 2 homolog (MDM2) and pVHL30. By undertaking a complementary approach, spanning from in silico analyses to yeast two-hybrid and mammalian cell assays, we defined the molecular details driving this novel interaction. Finally, we showed that a short intrinsically disordered segment of MDM2 is responsible for its association with pVHL in an isoform-specific fashion restricted to pVHL30.

Results

In silico protein–protein interacting network analysis identifies MDM2 as a novel interactor of pVHL. We previously documented a binary interaction between pVHL30 and p14ARF sustained by the acidic N-terminal tail of pVHL30, suggesting a functional asymmetry among pVHL isoforms[22]. p14ARF tumor suppressor is well known for its role in regulating p53 stability[24], sequestering MDM2 into a subnuclear compartment[25], while inhibiting p53 degradation[24]. p53 is also stabilized through pVHL[26]. In Zebrafish MDM2 degradation was regulated upon pVHL interaction with programmed cell death 5 protein (PDCD5), a negative regulator of MDM2. This evidence suggests a direct functional effect of pVHL loss of function on the p53/MDM2 pathway. To address this question, we used STRING to generate an interaction network centered on pVHL, HIF-1α, p14ARF, p53, and MDM2[27]. The resulting network was composed of twenty nodes connected by 52 edges, each of them representing an experimentally validated interaction (Fig. 1). The network is significantly more connected than expected by chance (p-value $< 1.0e^{-16}$), implying that these proteins are functionally interconnected. We asked whether non-trivial functional subnetworks can be linked to specific cell functions. We identified three distinct clusters formed by proteins linked to apoptosis, protein ubiquitination and hypoxia response. The first cluster was formed by six proteins, including p53, MDM2, and p14ARF. Gene ontology terms enrichment predicts this cluster to be mainly localized in the nucleus and participating in the regulation of transcription in response to hypoxia and cellular stress. The second cluster was composed of seven proteins, including pVHL, and, as expected, it was linked to protein degradation. The last cluster was the most heterogeneous and included proteins associated with both hypoxia- and stress-response, e.g. nutrient deprivation and viral aggression. Of note, we found a number of experimentally validated interactions connecting all of these three clusters, suggesting that the hypoxia response is functionally interconnected with cell cycle regulation. Manually curated enrichment of protein–protein interactions across network nodes further extended the connection between clusters I and II. Considering the concept of "interactors of interactors", a well-established property of protein–protein interaction networks[28,29] and the already validated physical interaction between pVHL, p53, and p14ARF, our in silico analysis predicts that MDM2 is a novel direct interactor of pVHL.

pVHL30 specifically interacts with MDM2. To validate the in silico-resolved pVHL association with MDM2, we used yeast two-hybrid (Y2H) assays. We tested whether pVHL binds to MDM2 in an isoform-specific fashion. To address this question, we generated vectors to express human MDM2 fused with Gal4-binding domain (Gal4-BD) as bait, and human pVHL30 and pVHL19 fused with Gal4-activation domain (Gal4-AD) as prey. Protein expression in yeast cells was verified by Western blotting (Figure S1). Transient expression of pVHL30, pVHL19, and MDM2 alone did not result in yeast growth in selective medium. On the other hand, co-expression of pVHL30 and MDM2 together resulted in increased yeast cell growth in selective medium, thereby

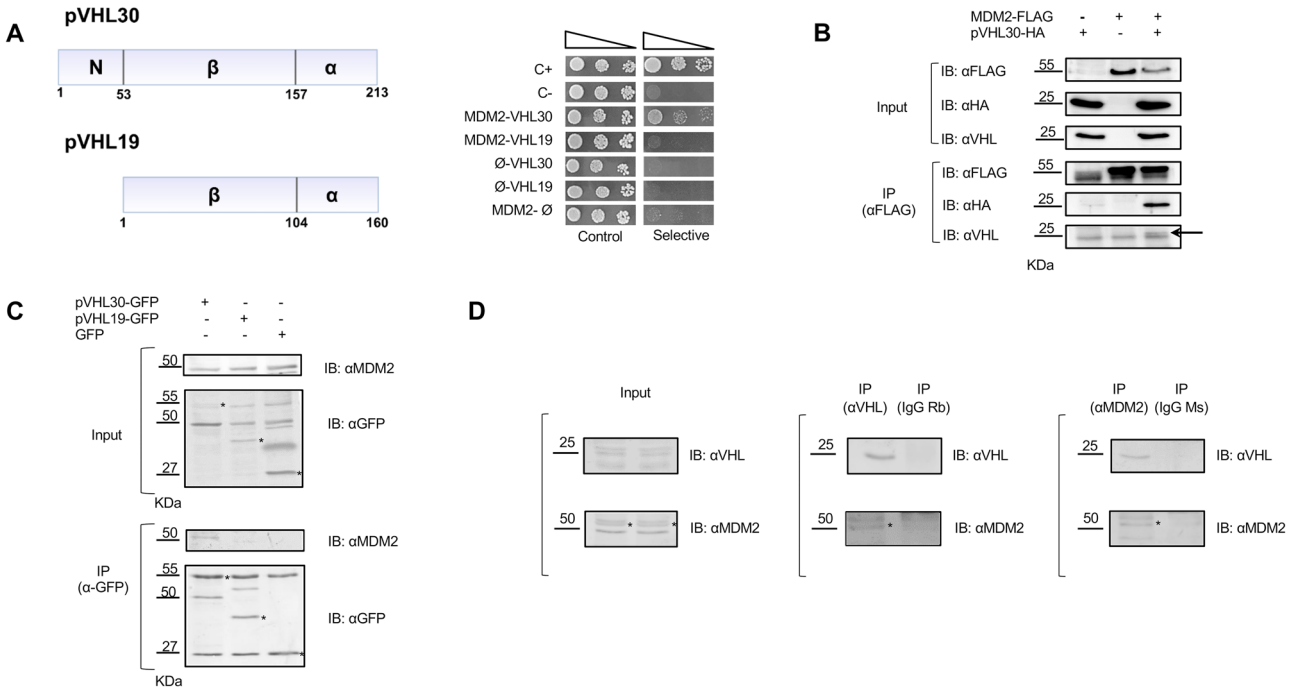

Figure 2. pVHL interacts with MDM2 is an isoform-specific manner. (**A**) Left panel: Schematic representation of pVHL30 and pVHL19 domains. The two isoforms differ for the presence of an intrinsically disordered N-terminus (N). Right panel: Y2H assay showing that pVHL30 specifically associates with MDM2. C+, positive control. C-, negative control (n = 10). (**B**) Immunoprecipitation (IP) of total protein extracts from HEK293T cells expressing Flag-MDM2 and HA-VHL30 with an anti-Flag antibody and immunostained with anti-Flag antibody, and anti-pVHL/anti-HA antibodies, as indicated. Arrow correspond to HA-VHL30 recognized by anti-VHL antibody (n = 3). (**C**) IP of total protein extracts from MN-1 cells expressing pVHL30-GFP, pVHL19-GFP, and soluble GFP, as indicated, and processed for pull down with anti-GFP antibody revealed endogenous MDM2 pull down only in the presence of pVHL30-GFP. Endogenous MDM2 was detected with a specific antibody. Asterisks indicate from left to right: pVHL30-GFP, pVHL19-GFP, and GFP both in input and Ip panels (n = 2). (**D**) IP of total protein extracts from HEK293T cells with either an anti-MDM2 antibody and IgG mouse as control or anti-pVHL antibody and IgG rabbit as control showed specific reciprocal pull down of endogenous proteins. Asterisks indicate the specific band corresponding to MDM2 protein (n = 3).

demonstrating the ability of MDM2 and pVHL30 to associate with each other in yeast cells (Fig. 2A and Figure S2). Although Y2H data cannot be considered quantitative per se, these results suggest a weak interaction, as the yeast growth rate was less sustained compared to the positive control. Importantly, co-expression of pVHL19 and MDM2 did not result in cell growth in selective medium, indicating that pVHL19 is unable to associate with MDM2 under these experimental conditions.

Next, we asked whether pVHL binds to MDM2 in an isoform-specific manner in mammalian cells. To test this hypothesis, we used human embryo kidney (HEK) 293 T cells transiently transfected with vectors expressing either HA-tagged pVHL30 (pVHL30-HA) or pVHL19-HA with Flag-tagged MDM2. Using immunoprecipitation and Western blotting analysis, we found that pVHL30 forms a complex with MDM2 (Fig. 2B and Figure S3). To determine whether pVHL30 binds endogenous MDM2 in an isoform-specific fashion, we generated vectors to express green fluorescent protein (GFP)-tagged pVHL30 (pVHL30-GFP) and pVHL19-GFP. Overexpression of pVHL30-GFP, and not pVHL19-GFP, in motor neuron-neuroblastoma hybrid MN-1 cells resulted in the pull down of endogenous MDM2 (Fig. 2C and Figure S4). Finally, we asked whether endogenous pVHL forms a complex with endogenous MDM2 (Fig. 2D and Figure S5). Immunoprecipitation of endogenous pVHL resulted in the pull down of endogenous MDM2. Notably, reciprocal immunoprecipitation of MDM2 specifically pulled down the pVHL isoform with the higher molecular weight, which corresponds to pVHL30. These observations indicate that pVHL30 specifically forms a complex with MDM2 in yeast as well as human- and mouse-derived mammalian cells. Moreover, our results suggest a functional role of the pVHL30 N-terminal tail in driving the interaction with MDM2.

MDM2 C-terminal domain binds to pVHL30. Next, we sought to determine which region of MDM2 specifically binds pVHL30. We generated vectors expressing MDM2 N-terminus (1–150), central acidic domain (151–350), and C-terminus (351–491) (Fig. 3A). By Western blotting we confirmed the expression of truncated MDM2 proteins in yeast (Figure S1). Yeast cells co-expressing pVHL30 together with the N-terminus or central acidic domain of MDM2 did not grow in selective medium, indicating no binding (Fig. 3B and Figure S6). Rather, yeast cells co-expressing pVHL30 and the MDM2 C-terminus grew in selective medium. These results indicate that the last 140 C-terminal residues of MDM2 (MDM2-CT, aa 351–491) are key for the pVHL30/

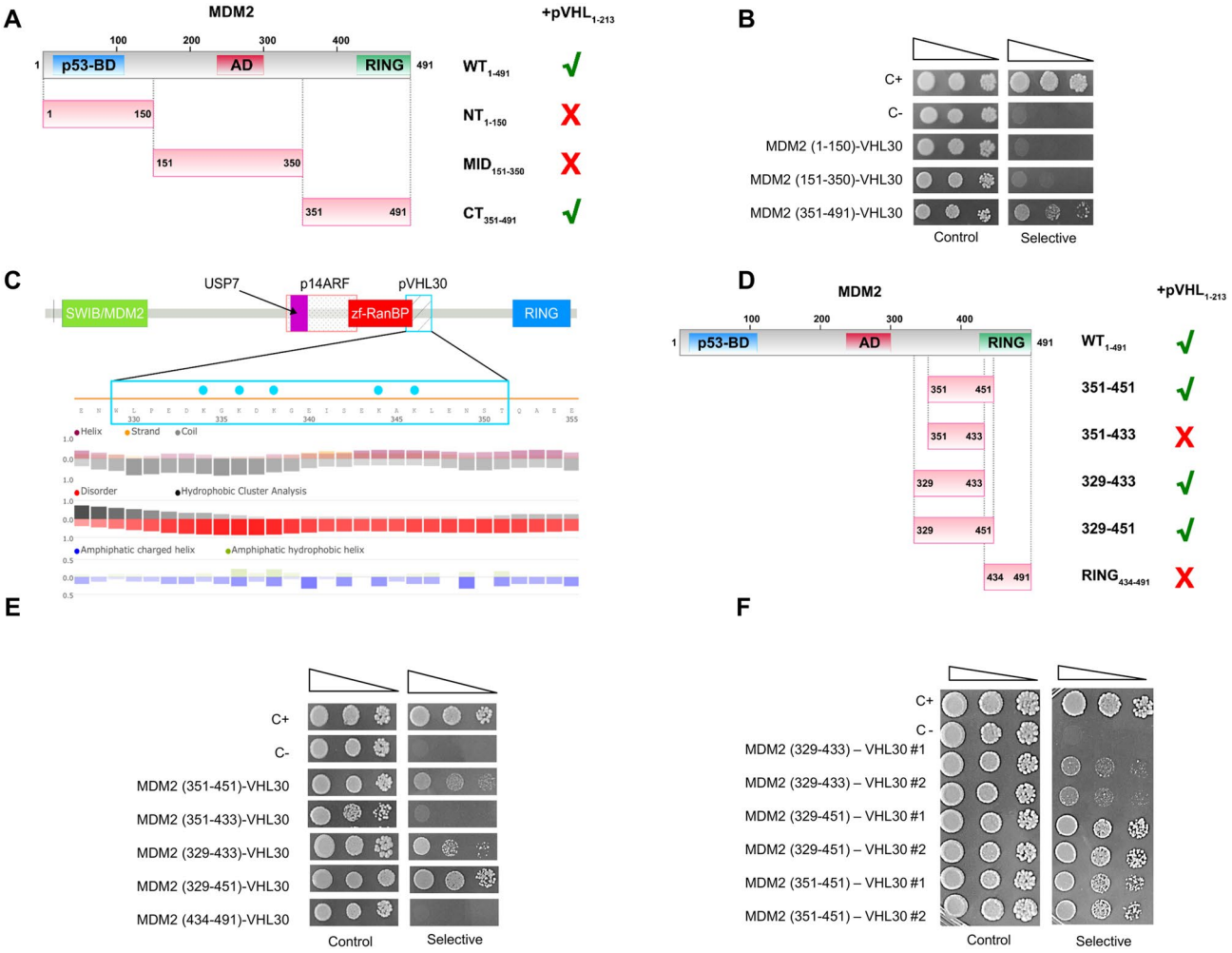

Figure 3. The intrinsically disordered portion of MDM2 is required for pVHL30 binding. (**A**) Schematic representation of MDM2 domain composition. (**B**) Y2H assays revealed that the C-terminal portion of MDM2 binds pVHL30. (n = 3). (**C**) Zoomed view and FELLS representation of the binding motif driving pVHL30/MDM2 association. Blue dots represent positively charged residues. The identified binding region partially overlaps the pseudo zinc-finger zf-RanBP. (**D**) Schematic representation of the C-terminal region MDM2 fragments used in panels (**E**,**F**). (**E**,**F**) Y2H assays revealed that the interaction of pVHL30 with MDM2 requires either the 329–350 or 434–451 regions of MDM2, yet the presence of the entire region (329–451) enhanced yeast growth (n = 3).

MDM2 interaction. Based on these observations we further characterized the C-terminal domain of MDM2. Analysis of the MDM2 primary structure with FELLS revealed hallmarks of an intrinsically disordered region spanning residues 329–433, terminating before the C3HC4-type zinc finger domain (RING, aa 434–491), which mediates MDM2 protein–protein and protein-RNA interactions[30–32] (Fig. 3C). By a Y2H assay, cells co-expressing both RING domain and pVHL30 did not grow in selective medium, indicating that the MDM2 RING domain does not associate with pVHL30 (Fig. 3D,E and Figure S7). Yeast cells co-expressing pVHL30 and the MDM2 351–433 fragment also failed to grow in selective medium. Elongation of the C-terminal end of this fragment to include the first part of the RING domain (MDM2 351–451) restored the interaction with pVHL30, despite the overall disruption of the RING domain structure. Collectively, these findings suggest that at least a portion of the RING domain mediates or modulates MDM2-pVHL30 association.

We thus wondered whether the MDM2 disordered region (aa 329–433) mediates the interaction with pVHL30, possibly by an additional and/or cooperative mechanism within the MDM2 C-terminus. Considering that the pVHL30 N-terminal tail, which is specifically involved in this interaction, is mostly acidic and characterized by the presence of eight GxEEx repetitions[22], we investigated whether clusters of positively charged residues within the MDM2 disordered region account for pVHL30 binding. In silico characterization with FELLS identified a region spanning residues 329–351 as a good candidate for pVHL30 binding (Fig. 3C). This region is predicted as fully disordered, with a typical alternation of charged residues. Of note, the position of a stretch of five lysine residues suggests these to form a positively charged cluster, which we hypothesize to form electrostatic interactions with the acidic pVHL30 N-terminus. In Y2H assay, co-expression of pVHL30 and the MDM2 329–433 fragment resulted in cell growth in selective medium, indicating that residues 329–433

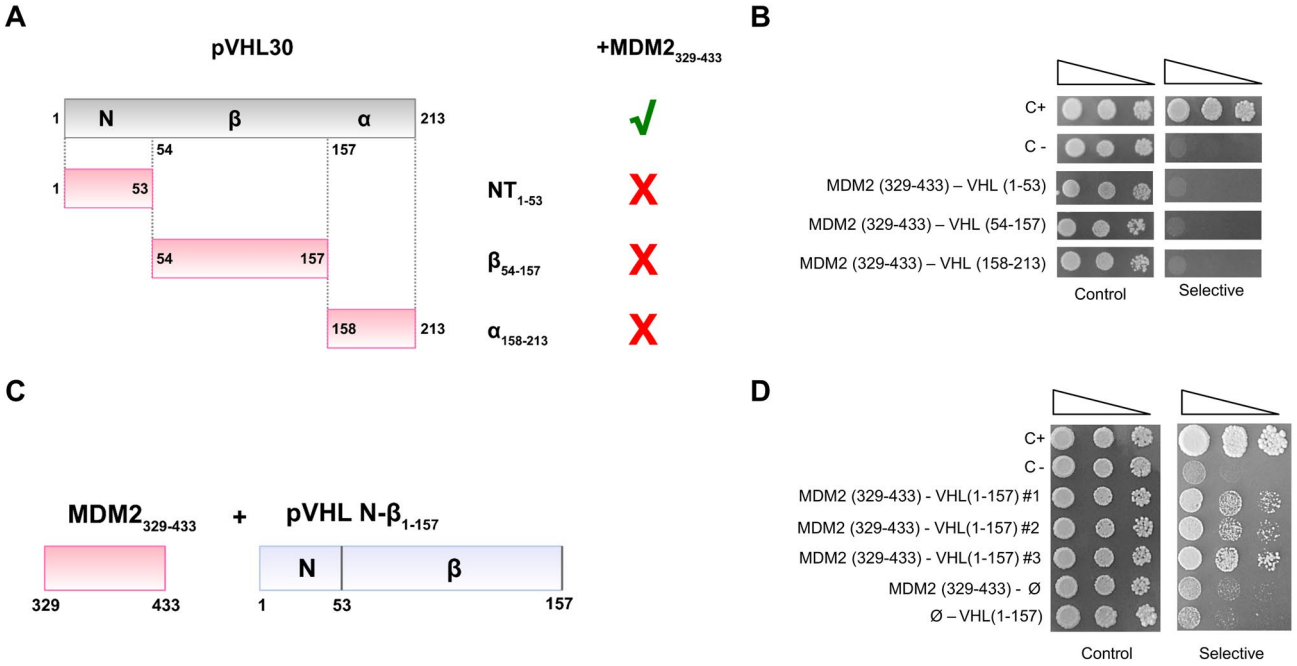

Figure 4. The N-terminus and β-domain of pVHL30 are required for MDM2 binding. (**A**) Schematic representation of pVHL30 domain composition. (**B**) Y2H assays revealed that none of pVHL30 domains alone bind MDM2 fragment 329–433 (n = 3). (**C**) Schematic representation of the MDM2 and pVHL30 fragments used in panel (**D**). (**D**) Y2H assays showed the interaction of pVHL30 1–157 region with MDM2 329–433 region (n = 3).

are the minimal MDM2 sequence required for interaction with pVHL30 (Fig. 3D,E and Figure S7). These data highlight the relevance of MDM2 residues 329–350 for binding, as interaction with pVHL30 is completely lost upon their removal. On the other hand, the stretch 329–350 was not sufficient for MDM2-pVHL30 interaction, as the MDM2 151–350 fragment was unable to bind pVHL30 (Fig. 3B). Interestingly, co-expressing pVHL30 with a longer MDM2 fragment (aa 329–451), which includes a portion of the RING domain implicated in the interaction (434–451), enhanced the growth rate of yeast cells in selective medium (Fig. 3E), supporting the idea that these two flanking sequences cooperatively improve the binding stability. To confirm this hypothesis, we further compared the growth of yeast cells co-expressing pVHL30 with MDM2 329–433, 329–451, and 351–451 fragments (Fig. 3F). Yeast cells grew more in presence of MDM2 329–451, pointing to a role of the flanking sequences to the binding stability/regulation.

The pVHL30 N-terminus and β-domain are required for interaction with MDM2. pVHL has multiple binding surfaces[33], each responsible for specific protein–protein interactions[34]. To identify the pVHL30 surface required for MDM2 binding, we generated yeast vectors expressing the pVHL N-terminus (aa 1–53), β-region (aa 54–157), and C-terminal α-domain (aa 158–213), and we performed Y2H assays (Figure S1). The N-terminus and β- and α-regions did not associate with MDM2 full length (Figure S8) and MDM2 329–433 fragment (Fig. 4A,B and Figure S9). These findings show that the pVHL30 N-terminal tail, although necessary (Fig. 2B), is not sufficient for MDM2 binding. Rather, our data suggest that pVHL30/MDM2 interaction is cooperatively driven by concurrent participation of the intrinsically disordered N-terminal tail and at least another pVHL30 domain. Consistent with this hypothesis, yeast cells expressing the pVHL30-N-β fragment (1–157) containing both the acid tail and ß-domain together with MDM2 329–433 fragment grew in selective medium, indicating that these portions of pVHL30 and MDM2 are critical binding surfaces required for such interaction (Fig. 4C,D). Taken together, this experimental evidence supports the idea that pVHL30/MDM2 interaction occurs through the MDM2 C-terminal region (aa 329–491) combining the binding of multiple interaction motifs within the 350–433 region to the pVHL-β domain. We propose that the pVHL30/MDM2 interaction relies on two factors, on one side the electrostatic interactions of the positively charged MDM2 residues (localized in the 329–350 stretch) with the negatively charged pVHL-N-terminus, and on the other side the positive contribution of (or part of) the RING domain.

Ab initio structure prediction and intrinsically disorder flavors characterization of MDM2 fragments. Limited structural information is available about the MDM2 region mediating the association with pVHL30 as no crystal structure is currently available for this region. Since intrinsically disordered regions, albeit lacking a fixed tertiary structure, are often associated with protein cellular function(s) depending on chemical property intrinsic to their primary structure[35–37], we investigated whether structural elements in MDM2 explain the different binding behaviors of MDM2 regions. To this aim, we performed ab initio structure prediction and disorder flavors characterization of the different MDM2 fragments tested in yeast. All predictions

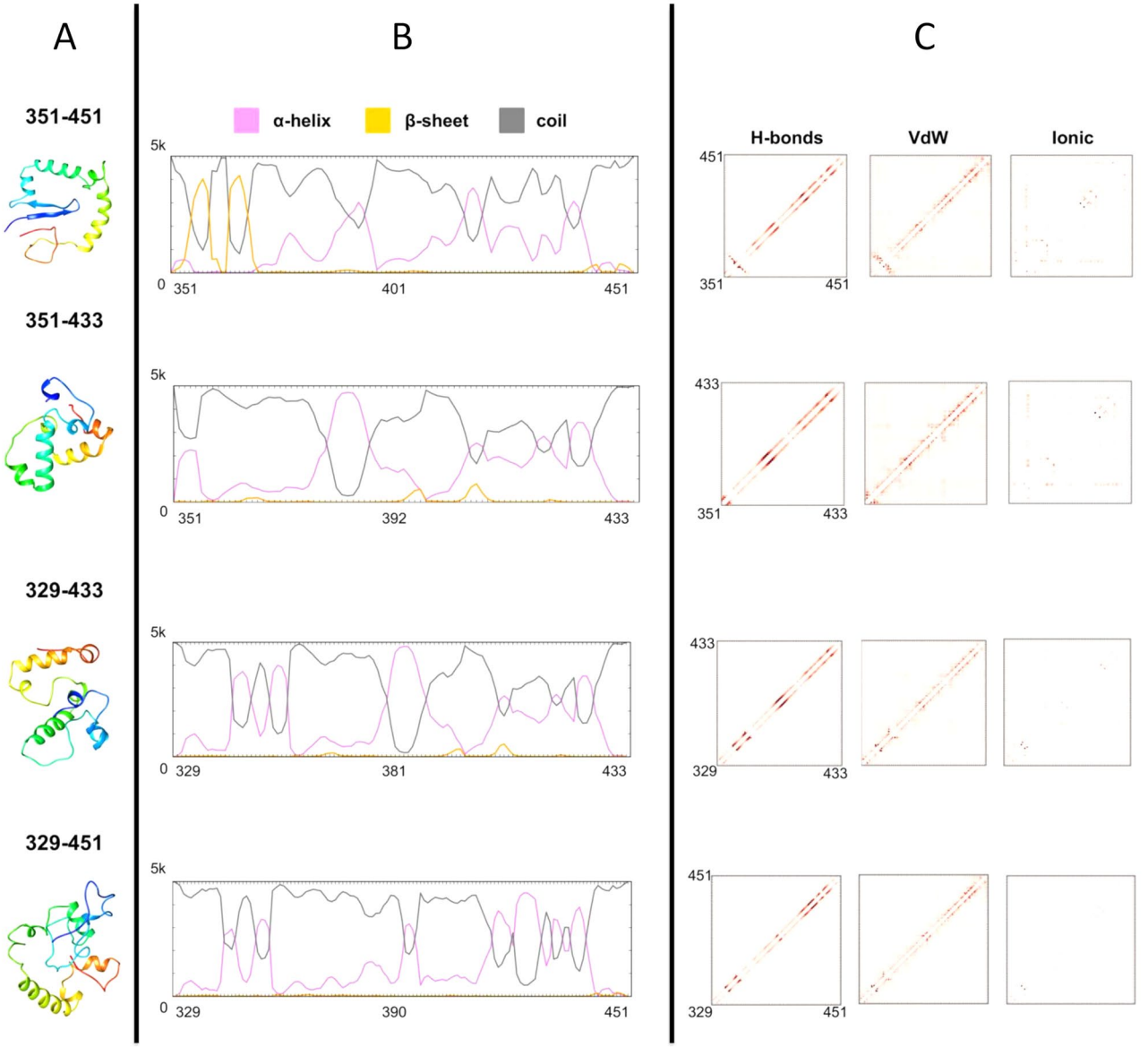

Figure 5. Characterization in silico of structural features of MDM2 fragments. Ab initio structure predictions (**A**), secondary structure content (**B**) and conserved intra-chains interactions (**C**) are presented for each fragment. The most probable 3D structures are presented as cartoon and colored rainbow with blue and red marking the N- and C-terminus respectively. Secondary structure content is calculated analyzing 5000 predictions is presented as plot. Intra-chain interactions describing network of interacting residues and type of interactions are presented as boxplots.

consistently showed that the MDM2 fragments spanning 351–451, 351–433, 329–433, and 329–451 are mostly disordered, with relevant differences in secondary structure content (Fig. 5A and Figure S10). The MDM2 351–451 fragment, containing the minimal sequences required for association with pVHL30, is characterized by a relatively high content of secondary structure. A small β-hairpin followed by a variable number of alpha bulges seems to be shared among different predictions. The β-hairpin is lost in predictions of MDM2 329–433 (which binds pVHL30), while alpha bulges are conserved. MDM2 329–451 is characterized by unfolded-like conformations albeit presenting few conserved secondary structure elements. On the other hand, the shorter MDM2 351–433 fragment, which lacks both flanking regions promoting MDM2-pVHL30 binding, is predicted as the most compact. Average secondary structure content, calculated upon 5000 3D structure predictions for each fragment, indicated that alpha bulges are conserved in both interacting and not interacting MDM2 fragments. These bulges mostly localize in the stretch 351–433, with flaking regions more frequently predicted as coil (Fig. 5B). Detailed characterization of residue-residue interactions for each model performed with RING[38] shows that the MDM2 351–433 (unable to bind pVHL30) is characterized by the highest hydrogen bonds, Van der Waals and ionic interactions (Fig. 5C). This finding supports the concept that this region, when isolated from flanking regions, acquires a more globular-like conformation. Conversely, on average the other fragments have comparable hydrogen bonds paired with a lower number of Van der Waals and ionic interactions, thus

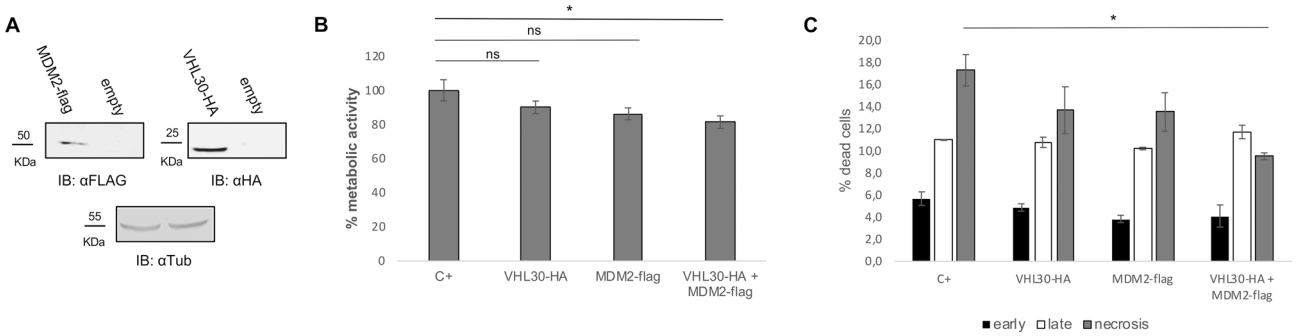

Figure 6. Gain of pVHL30 and MDM2 function reduces cell metabolism and cell necrosis. (**A**) Western blotting analysis of MN-1 cells transiently transfected with empty vector (mock) and vector expression either pVHL30-HA or MDM2-Flag, as indicated. (**B**) MTT assay in MN-1 cells transiently transfected as in (**A**) revealed that overexpression of both E3 ubiquitin ligases together significantly reduces cell metabolic activity (n = 16). (**C**) Propidium iodide (PI) and Annexin V analysis by flow cytometry after nutrient deprivation for 24 h showed that overexpression of MDM2-Flag and pVHL30-HA reduces cell necrosis (n = 3). Graphs, mean ± sem, ANOVA followed by Bonferroni post-hoc, *p < 0.05.

being relatively rich in secondary structure and more prone to adopt extended conformations. Collectively, all of these findings suggest that shortening MDM2 329–451, by removing both N- and C-flanking regions, stabilizes the polypeptide, thus lowering the intrinsically disordered behavior and inducing a conformational switch to order. Of note, multiple sequence alignment shows that the positively charged MDM2 329–351 region is maintained throughout evolution and is mostly conserved in Artiodactyla and Primates (Figure S11). As the number of acidic repeats forming pVHL30 N-terminal tail increases from rodents to primates[22], data suggest that the isoform-dependent MDM2/pVHL30 association could have specifically evolved in higher mammals. We further observed that the cluster of positive charges in region 329–351 appears counterbalanced by an opposed concentration of negative charges in region 410–433 (Figure S11), supporting the hypothesis that the two flanking sequences interact with the pVHL30 acidic N-terminus and β-domain, respectively, as pVHL β-domain presents a number of conserved positive residues mediating multiple protein–protein interactions[10,28,33]. Notably, MDM2 residues spanning 351–433 fragment includes six ATM (ataxia-telangiectasia mutated kinase) phosphorylation sites (i.e. S386, S395, S407, T419, S425, S429, Figure S11), strongly suggesting that post-translational modifications may operate as regulator of MDM2/pVHL30 association, e.g. introducing electrostatic repulsion against the pVHL30 acidic tail upon phosphorylation.

pVHL30 and MDM2 reduce cell metabolic activity and necrosis. To gain insights into the biological relevance of pVHL30/MDM2 interaction, we performed an MTT assay. Cell metabolic activity correlates with the rate of reduction of the tetrazolium salt to a purple formazan precipitate that occurs in metabolically active cells. We transiently transfected MN-1 cells with vectors expressing HA-tagged pVHL30 and Flag-tagged MDM2, and we verified exogenous protein expression by Western blotting (Fig. 6A). By MTT assay, we found that overexpression of either pVHL30 or MDM2 did not modify cell metabolism (Fig. 6B). Rather, co-expression of both E3 ubiquitin-protein ligases significantly reduced cell metabolic activity by 19%. Then, to evaluate whether the overexpression of HA-tagged pVHL30 and Flag-tagged MDM2 affects cell death, we analyzed apoptosis by flow cytometry using Annexin V and propidium iodide (Fig. 6C). We found no differences in early and late apoptosis as well as necrosis in the cells grown in normal conditions (data not shown). Nutrient deprivation for 24 h significantly reduced cell necrosis upon overexpression of both E3 ubiquitin ligases, suggesting a cooperative and synergistic effect of these E3 ubiquitin-protein ligases on cell metabolism and survival (Fig. 6C).

In summary, our results show an isoform-specific pVHL protein–protein structural and functional interaction. Together with our previous finding of pVHL30-p14ARF specific interaction[9,22], these observations support the idea that pVHL30 and the other isoforms have non-redundant functions in the cells.

Discussion

Functional intersections between oxygen sensing, apoptosis and cell cycle regulation are well described in the literature[26,28,39,40], although their functional inter-connection and mutual regulation are still debated. In particular, under prolonged hypoxia, p53 has been reported to accumulate in the cell, resulting in the direct repression of HIF-1α transcriptional activity[41]. A ternary complex between p53, HIF-1α, and MDM2 was proposed to promote pVHL-independent degradation of HIF-1α[39]. pVHL has been shown to directly associate with p53, thereby inducing both suppression of MDM2-mediated ubiquitination and nuclear export of p53[26]. Degradation of p53 is also regulated by p14ARF tumor suppressor[24], which inhibits the MDM2 E3 ubiquitin-protein ligase activity, leading to p53 accumulation and apoptosis[42]. Here, we describe a novel direct interaction between pVHL and MDM2. This association is pVHL30-isoform-specific and was observed in yeast and mammalian cells. Importantly, we provide evidence that this interaction occurs through the intrinsically disordered N-terminal tail of pVHL30, which indeed is not present in pVHL19. Notably, this acidic tail is necessary, but not sufficient for binding to MDM2, and it requires the pVHL β domain. This domain is known to engage a number of different protein–protein associations[34], and consistent with this idea it harbors the HIF-1α binding site. HIF-1α associates

with MDM2[39], an interaction thought to play a role in modulating hypoxia-induced p53 activation. Our data, while pointing out a novel interaction between MDM2 and pVHL30, suggest that pVHL30 and pVHL19 are characterized by different functional specializations. We speculate that transient macromolecular complexes composed of proteins participating in the regulation of both hypoxia sensing and cell cycle regulation may constantly be formed and destroyed in different cell compartments. Ideally, under mild hypoxia conditions the increased amount of free pVHL may trigger a pVHL30 functional relocation and MDM2 association. Of note, the MDM2 region that we found to participate in this association is immediately downstream of two overlapping binding sites for p14ARF (aa 210–304) and USP7 (aa 242–331), a deubiquitinating enzyme involved in p53 stabilization[43]. Within the MDM2 351–433 region, multiple phosphorylation sites for the ATM kinase are found to be relevant for activation of the DNA damage response[44]. Our data show that the pVHL30/MDM2 interaction is sustained by at least two linear interacting peptides (LIPs)[45] present on the MDM2 ab initio models and putatively modulated by either indirect (e.g. variation of oxygen concentration) and/or direct (e.g. site-specific phosphorylation) mechanisms. We show that overexpression of both pVHL30 and MDM2 reduces cell metabolic activity and, upon nutrient deprivation cell necrosis, suggesting activation of a specific metabolic reprogramming to escape stress condition. During the early cancer development, when the growing mass is still characterized by insufficient vascularization and diffused hypoxia, a similar behavior may lead to the selection of aggressive clones from heterogeneous tumor cells and promote a malignant progression[46]. Notably, during the revision of this manuscript, pVHL and MDM2 were shown to interact, leading to pVHL neddylation within a region crucial for the p53–pVHL interaction, preventing this association and induction of antiangiogenic factors[47]. Consistent with these observations, here we show for the first time that MDM2/pVHL interaction is isoform-specific. Thus, while pVHL30 is neddylated by MDM2, pVHL19 may not be a target of MDM2, further supporting isoform-specific functions, as we have previously proposed[22,28,48]. In a growing cancer environment, frequently characterized by heterogeneous clone population, the impact of hypoxic and nutritional stresses is amplified by both chaotic and insufficient neovasculature[49]. Considered this complex scenario, it is possible that different pVHL isoforms drive multiple modulation of the MDM2/p53/HIF-1α axis. On one hand, data about pVHL30/MDM2 interaction point to a starvation-induced adaptative role and modulation of angiogenesis. On the other hand, during sustained hypoxia pVHL19 can continue suppressing MDM2-mediated ubiquitination of p53, thus inducing cell cycle arrest and apoptosis[26]. In the context of transient complexes, the observations that a MDM2 motif driving its association with pVHL30 is immediately adjacent to other binding sites and can be modified by PTM is intriguing. It has been proposed that the interaction of pVHL30 with p14ARF induces its nuclear-to-nucleolar translocation, with concurrent dissociation of pVHL30 from the pVHL-elongin C-elongin B (VCB) complex[9]. A similar mechanism also triggers p14ARF-dependent functional inhibition of MDM2[42]. VCB-unbound pVHL30 can interact and stabilize p53 through its α-domain, by suppressing Mdm2-mediated ubiquitination as well as nuclear export[26,34]. Here, we demonstrated that both the N-terminal tail and β-domain are necessary for interaction with MDM2. Such kind of association involves different regions of the protein and is common among linear motif-mediated protein–protein interactions[50,51]. When bound to MDM2, pVHL30 may conceal ATM-specific phosphorylation sites yielding a further layer of regulation of MDM2 activity. Indeed, it has been already demonstrated that ATM induces p53 accumulation and activation by regulating MDM2 oligomerization[44], while pVHL associates with ATM impairing MDM2-mediated ubiquitination and p53 nuclear export[26]. Acting as a protein-hub, pVHL30 may concurrently form alternative ternary complexes under different conditions. The presence of an USP7 binding site in the same MDM2 region suggests that deubiquitination of several target proteins, such as MDM2 and p53, promotes their stabilization[43,52]. Consistent with this idea, other proteins can mediate USP7 association with p53[53]. In our recent investigation[22], we found two putative USP7 binding sites on the pVHL30 N-terminus (residues 35–44). Collectively, we propose that in addition to suggesting a novel HIF-1α independent function, the pVHL30 association with MDM2 may play a novel role in MDM2 stabilization and mutual regulation between oxygen sensing and apoptosis.

Methods

Bioinformatics analysis. A network of interacting proteins was built with Cytoscape[54] retrieving interaction data from STRING[27] (medium confidence 0.400), imposing no more than 5 interactors for the first shell and 10 for second shell. To reduce the number of false positive, text mining derived data were manually removed. The final network is composed of 20 nodes connected by 52 edges. The network shows an average node degree of 5.2 and an average local clustering coefficient of 0.721, with expected number of edges of 25. Human MDM2 and pVHL sequences were retrieved from UniProt[55] and visualized with Jalview[56]. Orthologous sequences were retrieved from OMA browser and aligned with a T-Coffee[57] (default parameters). Sequence features and secondary structure content were investigated with FELLS[58], functional domains mapped on the sequence using InterPro[59] and Pfam[60]. Linear motifs were predicted with ELM[61] and intrinsic disorder with MobiDB 3.0[62]. Ab initio protein structures prediction was performed with Rosetta 3.8[63] using specific protocol to model intrinsically disordered regions[64]. For each fragment 5000 decoys were generated and clustered using Rosetta clustering module. DSSP[65] was used to calculate secondary structure content for each 3D structure model, while networks of interacting residues were predicted with RING 2.0[38].

Plasmid constructs. The recombinant plasmids pGADVHL30, pGADVHL-Nt, pGADVHL-β and pcDNA3.1 HA-VHL30 were constructed as previously described[28]. Genes encoding the human MDM2 and pVHL30 proteins were obtained from commercial plasmid provided by GenScript (GenEZ plasmid OHu28568 and OHu23297) and cDNA transferred into pGBKT7 and pGADT7 plasmids (Clontech) to perform yeast two-hybrid assays (Y2H). PCR was used to amplify cDNAs using primers showed in Table S1 containing 15 nucleotides long 5′ ends addressing precise regions around EcoRI site in the MCS of both pGADT7 and pGBKT7

vectors. PCR obtained were cloned into pGADT7 or pGBKT7 linearized using EcoRI enzyme, following the In-Fusion HD Cloning Kit (Clontech) protocol. All Y2H recombinant plasmids constructed (Table S1) express the proteins in fusion with the Gal4 DNA binding domain (DBD) or the Gal4 DNA activation domain (AD) expressed by pGBKT7 and pGADT7, respectively. Chimeric proteins in yeast cells were revealed using anti HA and cMyc antibodies. GeneScript plasmid OHu28568 was directly used to overexpress MDM2 in mammalian cells, as the cDNA 5′-end is associated with the FLAG epitope. For Co-immunoprecipitation experiments, the pVHL30 and pVHL19 cDNAs sequences were cloned in the BamHI/EcoRI sites of the pcDNA3.1 vector, plus a N-terminal HA epitope sequence. The recombinant plasmids were used to overexpress pVHL30 and pVHL19 as N-terminal HA-tagged proteins. Sanger sequencing was used to verify all cloned sequences.

Yeast two-hybrid (Y2H) assays. The Matchmaker Gold Two Hybrid System (Clontech) was used to detect direct interaction between MDM2 and pVHL (default conditions). Positive interactions were revealed on multiple conditions by using selective medium lacking histidine and supplemented with 30, 60 or 90 mM 3-AT. Y190 cells were co-transformed with pGBKT7 and pGADT7 empty plasmids as negative control, whereas positive control expresses pGADT7-T (Gal4 AD-SV40 large T-antigen) and pGBKT7-53 (Gal4 DBD-murine p53, fragment 72–390). To exclude erroneous interpretation (i.e. auto-activation), Yeast Y190 cells co-expressing both fusion protein with Gal4 DBD and AD domain alone (and vice-versa) were tested. Expression of the Gal4-fusion proteins in yeast cells has been checked by Western blot analysis (Figure S1). For each transformation three independent clones were serially diluted (tenfold) and spotted either on solid selective medium lacking histidine (30 mM 3-AT and 60 mM 3-AT) or permissive medium, to check cell growth. Yeast strain growth was constantly monitored for 3–8 days at 30 °C. Total yeast proteins have been obtained by TCA-based solubilization of yeast cells[66], followed by standard Western Blot analysis[67], using either anti-HA (Abcam, ab16918), or anti-Myc (Abcam, ab127421) antibodies, to reveal the Gal4AD-pVHL or the Gal4BD-MDM2, respectively. Binding of two specific proteins is evaluated by co-expressing the proteins fused with either DNA-binding domain (bait), or the activation domain (prey), of the Gal4 transcription factor. Physical association between bait and prey allows activation of the reporter gene leading to the yeast cell growth on selective medium lacking histidine.

Transfection and co-immunoprecipitation from HEK293T cells. Co-immunoprecipitation experiments were performed using human kidney HEK293T cells provided by (Sigma-Aldrich). Cells were plated in a 1 ml well microplate and transfected at 70–80% confluence using Lipofectamine 2000 following the manufacturer protocols (Invitrogen). Each transfection was performed using approximately 10 µg of total DNA (i.e. pcDNA3.1-derived plasmids, empty and/or expressing either HA-pVHL30/pVHL19 or FLAG- MDM2. After 48 h, transfected cells were washed with phosphate-buffered saline (PBS) and lysed in lysis buffer (20 mM HEPES-Na pH7.4, 150 mM NaCl, 5 mM CHAPS) supplemented with 1X PIC (Protease Inhibitors Cocktail, Sigma). Cell lysates were centrifuged (10′ at 600 rpm, 4 °C) and the resulting post-nuclear supernatant (PNS) quantified by Bradford assay. For co-immunoprecitation, 0.2 mg of PNS were incubated for 4 h at 4 °C with 5 µl of protein A magnetic beads (Pierce Thermoscientific) pre-incubated (1 h at RT) with 2 µg of anti-FLAG antibody (Sigma, F7425). Immune complexes were finally washed 3 times with lysis buffer and eluted by incubating the beads (5′ at 70 °C) in 30 µl in 1X NuPAGE LDS sample buffer (Invitrogen) plus 0,1 M DTT. Both PNS and immunoprecipitated samples were separated by SDS–polyacrylamide gel electrophoresis and transferred to nitrocellulose membranes. The membranes were incubated with the anti-HA (Abcam, ab16918), anti-VHL (Santa Cruz, sc-5575) or anti-FLAG (Abcam, ab45766) antibodies to reveal the pVHL30/pVHL19 or MDM2, respectively. Additional Co-IPs were performed overexpressing GFP constructs in MN-1 cells and transfected with Lipofectamine2000 according to manufacturer protocol. Each transfection was performed using 2 µgr of pcDNA3.1-VHL30-GFP, pcDNA3.1-VHL19-GFP, and pcDNA3.1 GFP, respectively. All protocol steps are described above. In this case 400 µgr of PNS were incubated with 2 µg of anti-GFP (Abcam, ab1218). Following Western blot, membranes were incubated with anti MDM2 (Sigma, M7815) and anti GFP (Abcam, ab1218). Co-IPs of endogenous proteins were performed using 500 µgr of PNS incubated with 2 µg of anti-MDM2 or 1 µg of anti-VHL (Cell Signaling technology, 68,547). As control for specificity, we used 2 µg anti-IgG mouse (Millipore, 12-371B) and 1 µg anti-IgG rabbit (Millipore, PP64B). The following antibodies were used: Anti-GFP (Ab1218 Abcam, Ip), Anti-MDM2 (M7815 Sigma), Anti-VHL (68,547 Cell Signaling Technology).

MTT assay. Motor neuron-neuroblastoma hybrid MN-1 cells were seeded on 24-well plate and transfected at 70–80% confluence using Lipofectamine 2000 following manufacturer protocols (Invitrogen). After 48 h, 50 µl of MTT (Thiazolyl Blue Tetrazolium Bromide, code M5655 Sigma-5 mg/ml in PBS1X) was added to each well and the plate incubated for 10′ at 37 °C. Medium was eliminated, and DMSO was added to solubilize the water-insoluble MTT formazan crystals. The absorbance was recorded at 570 nm with spectrophotometer Nanodrop2000 (Thermo Fisher).

Propidium iodide and Annexin V assay. MN-1 cells were seeded on 6-well plate and transfected with Lipofectamine 2000 according to the manufacturer protocols. After 24 h culture medium was substituted with DMEM only to induce cell starvation. After 24 h 1×10^6 cells were resuspended in 100 µl of FACS buffer (DMEM no red phenol, FBS 0.1%, Hepes 12 mM) added with P.I 1:1000 (stock solution 1 mg/ml) and Annexin V 1:100 (Roche, Cat no. 118286810001). Samples were incubated dark at room temperature for 20 min and then analyzed by flow cytometry.

Data availability

The datasets generated during and/or analyzed during the current study are available from the corresponding author on reasonable request.

Code availability

UniProt accession numbers Q00987 and P40337 for the human MDM2 and pVHL proteins, respectively.

Received: 12 September 2019; Accepted: 6 September 2020
Published online: 28 September 2020

References

1. Wenger, R. H., Stiehl, D. P. & Camenisch, G. Integration of oxygen signaling at the consensus HRE. *Sci. STKE* **2005**, re12 (2005).
2. Welford, S. M. & Giaccia, A. J. Hypoxia and senescence: the impact of oxygenation on tumor suppression. *Mol. Cancer Res.* **9**, 538–544 (2011).
3. Nakazawa, M. S., Keith, B. & Simon, M. C. Oxygen availability and metabolic adaptations. *Nat. Rev. Cancer* **16**, 663–673 (2016).
4. Berra, E. *et al.* HIF prolyl-hydroxylase 2 is the key oxygen sensor setting low steady-state levels of HIF-1α in normoxia. *EMBO J.* **22**, 4082–4090 (2003).
5. Bruick, R. K. Oxygen sensing in the hypoxic response pathway: regulation of the hypoxia-inducible transcription factor. *Genes Dev.* **17**, 2614–2623 (2003).
6. Wang, G. L., Jiang, B. H., Rue, E. A. & Semenza, G. L. Hypoxia-inducible factor 1 is a basic-helix-loop-helix-PAS heterodimer regulated by cellular O2 tension. *Proc. Natl. Acad. Sci. U S A* **92**, 5510–5514 (1995).
7. Yang, J. *et al.* Functions of the Per/ARNT/Sim domains of the hypoxia-inducible factor. *J. Biol. Chem.* **280**, 36047–36054 (2005).
8. Bárdos, J. I. & Ashcroft, M. Negative and positive regulation of HIF-1: a complex network. *Biochem. Biophys. Acta.* **1755**, 107–120 (2005).
9. Lai, Y., Song, M., Hakala, K., Weintraub, S. T. & Shiio, Y. Proteomic dissection of the von Hippel-Lindau (VHL) interactome. *J. Proteome Res.* **10**, 5175–5182 (2011).
10. Hon, W.-C. *et al.* Structural basis for the recognition of hydroxyproline in HIF-1 alpha by pVHL. *Nature* **417**, 975–978 (2002).
11. McDonough, M. A. *et al.* Cellular oxygen sensing: crystal structure of hypoxia-inducible factor prolyl hydroxylase (PHD2). *Proc. Natl. Acad. Sci. U.S.A.* **103**, 9814–9819 (2006).
12. Metzen, E. *et al.* Regulation of the prolyl hydroxylase domain protein 2 (phd2/egln-1) gene: identification of a functional hypoxia-responsive element. *Biochem. J.* **387**, 711–717 (2005).
13. Chowdhury, R. *et al.* Structural basis for binding of hypoxia-inducible factor to the oxygen-sensing prolyl hydroxylases. *Structure* **17**, 981–989 (2009).
14. Minervini, G. *et al.* Design and analysis of a Petri net model of the Von Hippel-Lindau (VHL) tumor suppressor interaction network. *PLoS ONE* **9**, e96986 (2014).
15. Pugh, C. W. & Ratcliffe, P. J. Regulation of angiogenesis by hypoxia: role of the HIF system. *Nat. Med.* **9**, 677–684 (2003).
16. Latif, F. *et al.* Identification of the von Hippel-Lindau disease tumor suppressor gene. *Science* **260**, 1317–1320 (1993).
17. Iliopoulos, O., Kibel, A., Gray, S. & Kaelin, W. G. Tumour suppression by the human von Hippel-Lindau gene product. *Nat. Med.* **1**, 822–826 (1995).
18. Maher, E. R., Neumann, H. P. & von Richard, S. Hippel-Lindau disease: a clinical and scientific review. *Eur. J. Hum. Genet.* **19**, 617–623 (2011).
19. Minervini, G., Quaglia, F., Tabaro, F. & Tosatto, S. C. E. Genotype-phenotype relations of the von Hippel-Lindau tumor suppressor inferred from a large-scale analysis of disease mutations and interactors. *PLoS Comput. Biol.* **15**, e1006478 (2019).
20. Kaelin, W. G. Molecular basis of the VHL hereditary cancer syndrome. *Nat. Rev. Cancer* **2**, 673–682 (2002).
21. Iliopoulos, O., Ohh, M. & Kaelin, W. G. pVHL19 is a biologically active product of the von Hippel-Lindau gene arising from internal translation initiation. *Proc. Natl. Acad. Sci. U.S.A.* **95**, 11661–11666 (1998).
22. Minervini, G. *et al.* Isoform-specific interactions of the von Hippel-Lindau tumor suppressor protein. *Sci. Rep.* **5**, 12605 (2015).
23. Hascoet, P. *et al.* The pVHL172 isoform is not a tumor suppressor and up-regulates a subset of pro-tumorigenic genes including TGFB1 and MMP13. *Oncotarget* https://doi.org/10.18632/oncotarget.18376 (2017).
24. Xirodimas, D., Saville, M. K., Edling, C., Lane, D. P. & Laín, S. Different effects of p14ARF on the levels of ubiquitinated p53 and Mdm2 in vivo. *Oncogene* **20**, 4972–4983 (2001).
25. Weber, J. D., Taylor, L. J., Roussel, M. F., Sherr, C. J. & Bar-Sagi, D. Nucleolar Arf sequesters Mdm2 and activates p53. *Nat Cell Biol* **1**, 20–26 (1999).
26. Roe, J.-S. *et al.* p53 stabilization and transactivation by a von Hippel-Lindau protein. *Mol. Cell* **22**, 395–405 (2006).
27. Szklarczyk, D. *et al.* The STRING database in 2017: quality-controlled protein–protein association networks, made broadly accessible. *Nucleic Acids Res* **45**, D362–D368 (2017).
28. Minervini, G. *et al.* Novel interactions of the von Hippel-Lindau (pVHL) tumor suppressor with the CDKN1 family of cell cycle inhibitors. *Sci. Rep* **7**, 46562 (2017).
29. Tenga, M. J. & Lazar, I. M. Proteomic study reveals a functional network of cancer markers in the G1-Stage of the breast cancer cell cycle. *BMC Cancer* **14**, 710 (2014).
30. Elenbaas, B., Dobbelstein, M., Roth, J., Shenk, T. & Levine, A. J. The MDM2 oncoprotein binds specifically to RNA through its RING finger domain. *Mol Med* **2**, 439–451 (1996).
31. Linares, L. K., Hengstermann, A., Ciechanover, A., Müller, S. & Scheffner, M. HdmX stimulates Hdm2-mediated ubiquitination and degradation of p53. *Proc. Natl. Acad. Sci. U.S.A.* **100**, 12009–12014 (2003).
32. Challen, C., Anderson, J. J., Chrzanowska-Lightowlers, Z. M. A., Lightowlers, R. N. & Lunec, J. Recombinant human MDM2 oncoprotein shows sequence composition selectivity for binding to both RNA and DNA. *Int. J. Oncol.* **40**, 851–859 (2012).
33. Leonardi, E., Murgia, A & Tosatto, S. C. E. Adding structural information to the von Hippel-Lindau (VHL) tumor suppressor interaction network. *FEBS Lett.* **583**, 3704–10 (2009).
34. Tabaro, F. *et al.* VHLdb: A database of von Hippel-Lindau protein interactors and mutations. *Sci. Rep.* **6**, 31128 (2016).
35. Vucetic, S., Brown, C. J., Dunker, A. K. & Obradovic, Z. Flavors of protein disorder. *Proteins* **52**, 573–584 (2003).
36. Necci, M., Piovesan, D. & Tosatto, S. C. E. Large-scale analysis of intrinsic disorder flavors and associated functions in the protein sequence universe. *Protein Sci.* https://doi.org/10.1002/pro.3041 (2016).
37. Piovesan, D. *et al.* DisProt 7.0: a major update of the database of disordered proteins. *Nucleic Acids Res.* **45**, D1123–D1124 (2017).
38. Piovesan, D., Minervini, G. & Tosatto, S. C. E. The RING 2.0 web server for high quality residue interaction networks. *Nucleic Acids Res.* (2016) https://doi.org/10.1093/nar/gkw315.
39. Chen, D., Li, M., Luo, J. & Gu, W. Direct interactions between HIF-1α and Mdm2 modulate p53 function. *J. Biol. Chem.* **278**, 13595–13598 (2003).
40. Roe, J.-S. & Youn, H.-D. The positive regulation of p53 by the tumor suppressor VHL. *Cell Cycle* **5**, 2054–2056 (2006).

41. Ravi, R. *et al.* Regulation of tumor angiogenesis by p53-induced degradation of hypoxia-inducible factor 1α. *Genes Dev* **14**, 34–44 (2000).
42. Sherr, C. J. Divorcing ARF and p53: an unsettled case. *Nat Rev Cancer* **6**, 663–673 (2006).
43. Li, M. *et al.* Deubiquitination of p53 by HAUSP is an important pathway for p53 stabilization. *Nature* **416**, 648–653 (2002).
44. Cheng, Q., Chen, L., Li, Z., Lane, W. S. & Chen, J. ATM activates p53 by regulating MDM2 oligomerization and E3 processivity. *EMBO J.* **28**, 3857–3867 (2009).
45. Piovesan, D. & Tosatto, S. C. E. Mobi 2.0: an improved method to define intrinsic disorder, mobility and linear binding regions in protein structures. *Bioinformatics* **34**, 122–123 (2018).
46. García-Jiménez, C. & Goding, C. R. Starvation and pseudo-starvation as drivers of cancer metastasis through translation reprogramming. *Cell Metab.* **29**, 254–267 (2019).
47. Wolf, E. R., Mabry, A. R., Damania, B. & Mayo, L. D. Mdm2-mediated neddylation of pVHL blocks the induction of antiangiogenic factors. *Oncogene* **39**, 5228–5239 (2020).
48. Minervini, G., Pennuto, M. & Tosatto, S. C. E. The pVHL neglected functions, a tale of hypoxia-dependent and -independent regulations in cancer. *Open Biol.* **10**, 200109.
49. Nagy, J. A., Chang, S.-H., Dvorak, A. M. & Dvorak, H. F. Why are tumour blood vessels abnormal and why is it important to know?. *Br. J. Cancer* **100**, 865–869 (2009).
50. Dinkel, H. *et al.* ELM 2016–data update and new functionality of the eukaryotic linear motif resource. *Nucleic Acids Res.* **44**, D294-300 (2016).
51. Brandmann, T. *et al.* Molecular architecture of LSM14 interactions involved in the assembly of mRNA silencing complexes. *EMBO J.* **37**, e97869 (2018).
52. Li, M., Brooks, C. L., Kon, N. & Gu, W. A dynamic role of HAUSP in the p53-Mdm2 pathway. *Mol. Cell* **13**, 879–886 (2004).
53. Zhang, J. *et al.* ABRO1 suppresses tumourigenesis and regulates the DNA damage response by stabilizing p53. *Nat. Commun* **5**, 5059 (2014).
54. Shannon, P. *et al.* Cytoscape: a software environment for integrated models of biomolecular interaction networks. *Genome Res.* **13**, 2498–2504 (2003).
55. UniProt: a worldwide hub of protein knowledge. *Nucleic Acids Res* **47**, D506–D515 (2019).
56. Waterhouse, A. M., Procter, J. B., Martin, D. M. A., Clamp, M. & Barton, G. J. Jalview Version 2–a multiple sequence alignment editor and analysis workbench. *Bioinformatics* **25**, 1189–1191 (2009).
57. Notredame, C., Higgins, D. G. & Heringa, J. T-coffee: A novel method for fast and accurate multiple sequence alignment. *J. Mol. Biol.* **302**, 205–217 (2000).
58. Piovesan, D., Walsh, I., Minervini, G. & Tosatto, S. C. E. FELLS: fast estimator of latent local structure. *Bioinformatics* https://doi.org/10.1093/bioinformatics/btx085 (2017).
59. Mitchell, A. L. *et al.* InterPro in 2019: improving coverage, classification and access to protein sequence annotations. *Nucleic Acids Res.* **47**, D351–D360 (2019).
60. El-Gebali, S. *et al.* The Pfam protein families database in 2019. *Nucleic Acids Res* **47**, D427–D432 (2019).
61. Gouw, M. *et al.* The eukaryotic linear motif resource:2018 update. *Nucleic Acids Res* **46**, D428–D434 (2018).
62. Piovesan, D. *et al.* MobiDB 3.0: more annotations for intrinsic disorder, conformational diversity and interactions in proteins. *Nucleic Acids Res.* **46**, D471–D476 (2018).
63. Leaver-Fay, A. *et al.* ROSETTA3: an object-oriented software suite for the simulation and design of macromolecules. *Meth. Enzymol.* **487**, 545–574 (2011).
64. Wang, R. Y.-R. *et al.* Modeling disordered regions in proteins using Rosetta. *PLoS One* **6**, (2011).
65. Kabsch, W. & Sander, C. Dictionary of protein secondary structure: pattern recognition of hydrogen-bonded and geometrical features. *Biopolymers* **22**, 2577–2637 (1983).
66. Wright, A. P., Bruns, M. & Hartley, B. S. Extraction and rapid inactivation of proteins from *Saccharomyces cerevisiae* by trichloroacetic acid precipitation. *Yeast* **5**, 51–53 (1989).
67. Evans, G. A. Molecular cloning: a laboratory manual. Second edition. Volumes 1, 2, and 3. Current protocols in molecular biology. Volumes 1 and 2. *Cell* **61**, 17–18 (1990).

Acknowledgements

This work was supported by Associazione Italiana per la Ricerca sul Cancro (AIRC) grant IG 2015 ID. 17753 and IG 2019 ID. 23825 to ST. Telethon-Italy Grant GGP19128 to M.P. The funders had no role in study design, data collection and analysis, decision to publish, or preparation of the manuscript.

Author contributions

G.M., R.L., G.S., M.P., S.T. conceived the experiments. AF, GM, RB and DP performed the experiments. A.F., G.M., G.S., R.L., analyzed the data. G.M., R.L., G.S., M.P. and S.T. wrote the manuscript.

Competing interests

The authors declare no competing interests.

Additional information

Supplementary information is available for this paper at https://doi.org/10.1038/s41598-020-72683-3.

Correspondence and requests for materials should be addressed to S.C.E.T.

Reprints and permissions information is available at www.nature.com/reprints.

Publisher's note Springer Nature remains neutral with regard to jurisdictional claims in published maps and institutional affiliations.